Influence of the Molecular Ordering on the Wetting of SiO_2/Air Interfaces by Alkanes

C. Merkl, T. Pfohl, and H. Riegler

Max-Planck-Institut für Kolloid- und Grenzflächenforschung, Rudower Chaussee 5, D-12489 Berlin, Germany

(Received 21 January 1997)

Alkanes from 16 to 50 C atoms show three wetting topologies at SiO_2/air interfaces. Below the bulk freezing temperature T_b, small crystallites (frozen droplets which can be annealed into mesas of uniform height) are observed. A monolayer of homeotropically oriented molecules covers the air/substrate interface in between. At T_b, the crystallites melt into droplets. The ordered monolayer remains up to $T_S^{SV} \approx T_b + 3\,°C$, probably due to fluctuation-stabilized "surface freezing." Above T_S^{SV}, a liquid alkane film wets the surface. The decoupling of T_b and T_S^{SV}, and the difference between the ordered and liquid surface energies, causes the droplet-to-film transition. [S0031-9007(97)04693-0]

PACS numbers: 68.45.Gd, 68.55.Jk

Wetting is governed by interfacial interactions [1,2], which can efficiently be studied by the use of liquid hydrocarbons. Their interactions are dominated by long range dispersion forces which can be tuned by changing their conformation or chain length. Appropriate solid surfaces for wetting studies are chemically and physically well defined silicon wafer surfaces. With such systems, particularly, the contribution of long range dispersion forces has been investigated [3–5]. In general, however, wetting is determined by long and short range forces [6–8]. Even for alkanes, local interactions are explicit through surface freezing, i.e., the bulk liquid/vapor interface is covered with an ordered alkane monolayer up to several °C above the bulk melting temperature [9,10]. In the following, we will show that surface freezing of alkanes also occurs at solid/vapor interfaces and that it has a significant impact on the wetting behavior.

The alkanes ($C_nH_{2n+2} := C_n$) were used as purchased [Aldrich, C_{50} and C_{60} from Fluka, purity >99% (C_{50} > 98%)]. Pieces of silicon wafers (Wacker Siltronic GmbH, Burghausen, oxide layer thickness ≈15 Å) served as substrates. The SiO_2 surfaces were prepared as described elsewhere [11]. Ultrathin alkane films were made with equivalent results by spincoating either from chloroform solutions or alkane melts. Deposition parameters were selected to deposit material sufficient for average surface coverages of several hundred Å. The samples were studied via reflection optical microscopy (Olympus AX70), x-ray reflectivity (Stoe Θ/Θ reflectometer), and ellipsometry (Beaglehole Instruments). The ellipsometry and x-ray data analysis is described elsewhere [10,12]. The homemade temperature stages (accuracy ≈0.1 °C) were calibrated with the alkane bulk melting temperatures, which were separately checked via differential scanning calorimetry to match literature values. Some experiments with short chain alkanes, performed under saturated alkane vapor atmosphere, show that evaporation losses do not affect the results.

For chain lengths C_{16} through C_{50}, optical microscopy studies reveal three different wetting topologies (Fig. 1) with transition temperatures at the bulk melting temperature T_b [13] and at T_S^{SV}, slightly above T_b (Fig. 2). For chain lengths below C_{16} and above C_{50}, respectively, only the two topologies typical for $T < T_b$ and $T > T_S^{SV}$ are observed.

Below T_b, depending on the state of annealing, the crystalline material is clustered either as frozen droplets, as frozen droplets with pedestals of smooth, planar surfaces, or as mesalike crystallites (islands), which also have smooth, planar surfaces. The interference colors and atomic force microscopy data indicate that the mesas and pedestals have similar heights (≈500 Å). Annealing at temperatures just below T_b induces the pedestals to grow in area at constant height. The alkane material is supplied from the center droplet, which decreases in size.

Between T_b and T_S^{SV}, droplets are observed (occasionally distorted by pinning, e.g., dust particles). Their interference colors vary continuously indicating smooth spherical caps. Evidently they are composed of liquid alkane, consistent with the microscopically observed melting behavior at T_b. From the droplet diameter $2r$ and the number i of interference fringes [$h \approx i\lambda/2n$, $\lambda =$ 500 nm, $n =$ refractive index (1.45)], the contact angle Θ_d can be estimated

$$\Theta_d = \sin^{-1}\left(\frac{2rh}{r^2 + h^2}\right). \quad (1)$$

Θ_d depends on the temperature. Roughly independent from the chain length, it decreases from ≈10° near T_b to ≈2° near T_S^{SV} [14]. At constant temperature, Θ_d does not change with time.

Above T_S^{SV}, we observe either structureless, smooth surfaces if only small amounts of material were deposited, or, with a higher alkane surface coverage, very flat droplets with noncircular, smoothly curved shapes. In the latter case, the contact angle is very small and the topology is very susceptible to distortion by pinning.

The analysis [12] of the x-ray reflectivity data (Fig. 3) reveals below T_S^{SV} (i.e., in the mesa and in the droplet regime) thin films (electron density ≈0.31 ± 0.03 $e/Å^3$). These films are evident even without sophisticated analysis

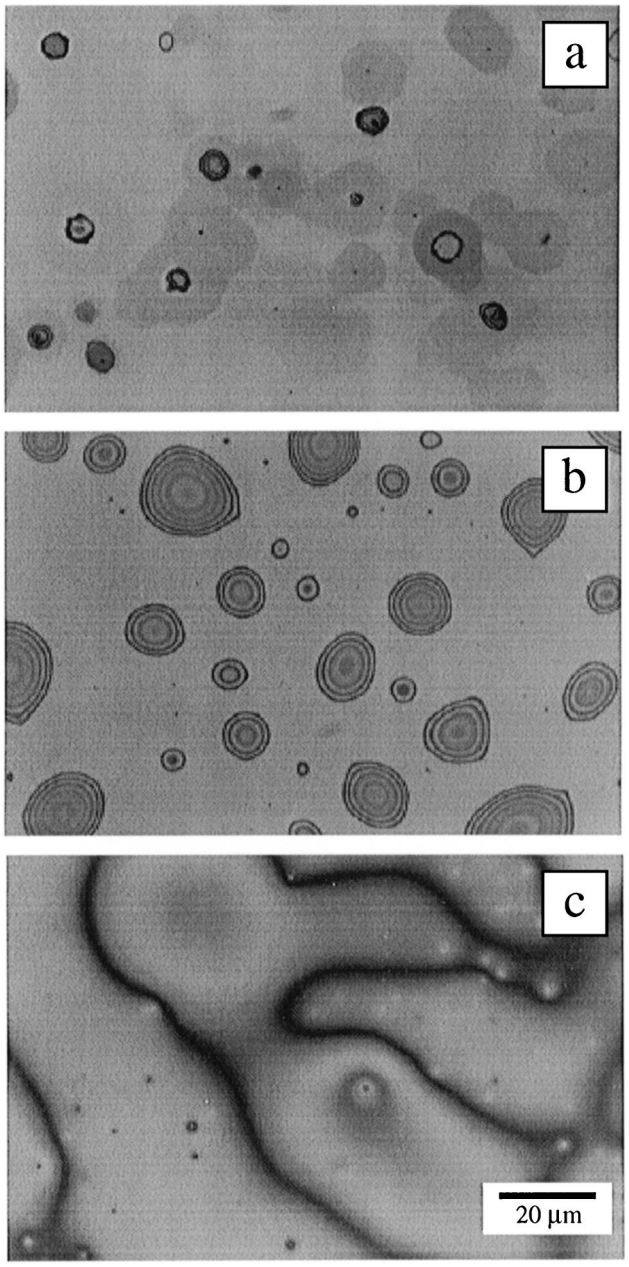

FIG. 1. Optical microscopy images of C_{30} in the three wetting topologies ($T_b = 66.1\,°C$, $T_S^{SV} = 69.3\,°C$). (a) $T = 65.0\,°C$; (b) $T = 68.0\,°C$; (c) $T = 70.0\,°C$.

from the interference minima ("Kiessig fringes"). Their thicknesses scale with the alkane length. For $C_n < C_{30}$, they are slightly thicker ($\approx$10%) than one all-trans-molecular length. For $C_n > C_{30}$, they roughly match the length. Detailed studies [14] reveal even/odd effects and minor thickness changes at T_b. All of this indicates that the films consist of densely packed ("frozen") alkanes, oriented normal to the interface, which will, henceforth, be termed "monolayers." These monolayers are at the SiO_2/air interface. The mesas, which are much thicker, do not contribute to the monolayer interferences [15] and

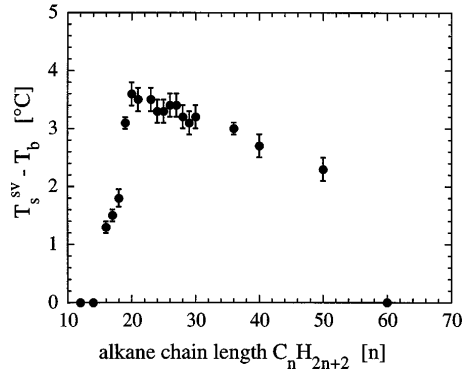

FIG. 2. Difference between the droplet/film transition temperature T_S^{SV} and the bulk freezing temperature T_b as a function of the alkane chain length.

the liquid droplets do not produce interferences at all due to their curved surfaces.

Above T_S^{SV}, x-ray interferences also reveal smooth films. If the amount of deposited material is sufficient only for films of less than $\approx$160 Å thickness, the sample surface appears smooth under the microscope. Reflectivity shows films with thicknesses roughly proportional to the amount of deposited material. With more deposited

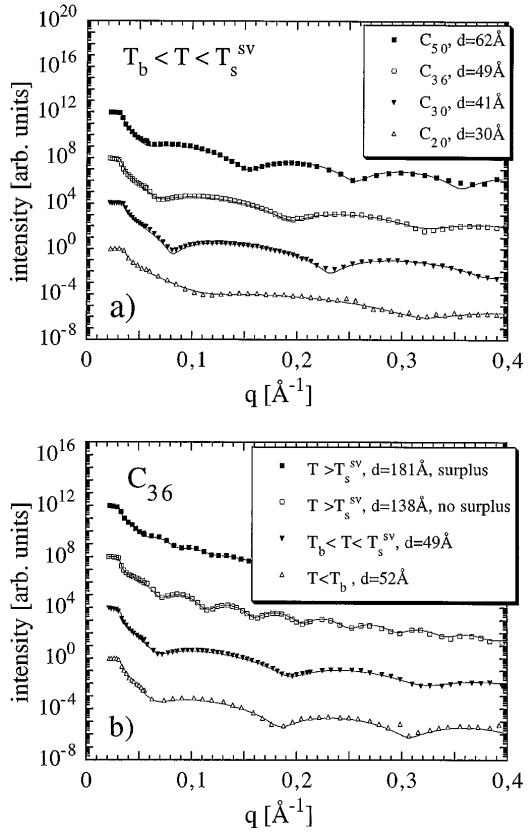

FIG. 3. X-ray reflectivity data ($q = 4\pi/\lambda \sin\Theta$, Θ = grazing angle, $\lambda = 1.54$ Å) of (a) alkanes of various chain lengths at $T_b < T < T_S^{SV}$ and (b) C_{36} on SiO_2 at various temperatures. The solid lines show fits from which the layer thicknesses are derived.

material, microscopy reveals the accumulation of the "surplus" of material beyond 160–200 Å film thickness in very flat droplets. X-ray reflectivity still reveals a spacing of 160–200 Å. This probably originates from a film between the flat droplets because the interferences disappear with increasing droplet coverage. The film consists of liquid alkane because its thickness is independent from the alkane chain length, no x-ray interferences due to any internal molecular layering are observed, and because of its electron density ($0.24 \pm 0.03\ e/\text{Å}^3$). The film is also apparent from optical microscopy observations. Upon cooling below T_S^{SV}, droplets are formed even from smooth films thinner than 160 Å, or, in the surplus case, in the areas between the flat droplets.

The topologies are reversible (except for the transformation of the frozen droplets into mesas). Upon cooling, temperature hysteresis is observed. Upon heating, no hysteresis is found (T_b and T_S^{SV} are defined in heating experiments). Temperature variation within the various wetting regimes does not change their general wetting topologies.

Scattering and interference effects spoiled ellipsometric studies with spincoated films. Therefore, adsorption experiments from saturated vapor phases were performed with C_{20}. These resulted in smooth films. Figure 4 shows that their ellipticity, which is roughly proportional to the adsorbed amount [10], changes abruptly at T_S^{SV}. No changes are detected at T_b. Below T_S^{SV}, both the ellipsometric data and the x-ray reflectivity measurements (*from the same samples*) reveal a film thickness comparable to that of monolayers of spincoated samples. Above T_S^{SV}, within a wide temperature range, the layer thickness is constantly about half a molecular length (≈15 Å). The discrepancy to the 160–200 Å films measured with x-rays on spincoated samples is tentatively attributed to an incomplete saturation of the vapor phase in the adsorption experiment.

The various experimental results show a change in the wetting behavior at T_b and T_S^{SV}. At the bulk freezing temperature T_b, this can be expected. However, to the best of our knowledge, the bulk properties do not change abruptly at T_S^{SV}. Hence, it is suggested that the wetting transition at T_S^{SV} is due to a discontinuity in the interfacial molecular ordering.

The chain length and temperature dependency of T_S^{SV} resembles that of the surface freezing temperature of alkane monolayers at bulk alkane/air interfaces T_S^{LV} [9,10]. However, T_S^{LV} is on average 0.3–0.5 °C lower than T_S^{SV}, and γ^{LV} does not change discontinuously at T_S^{LV} or T_S^{SV} (see inset in Fig. 5). Hence, surface freezing at the droplet/air interface is not causing the transition. On the other hand, a discontinuous change of the molecular ordering at the bulk alkane/substrate interface at T_S^{SV} (i.e., of γ^{SL}) cannot be excluded with any degree of certainty, because neither x-ray reflectivity nor microscopy provided information on the molecular ordering at this interface in the droplet or film regime. Nevertheless, the x-ray and ellipsometric measurements prove an abrupt change of the molecular ordering at the air/substrate interface exactly at T_S^{SV} suggesting a change in γ^{SV} as a major cause of the transition.

Equilibrium presumed, we may write

$$\begin{aligned} \gamma_f^{SV} &= \gamma_f^{LV} \cos\Theta_f + \gamma_f^{SL}; \\ \gamma_d^{SV} &= \gamma_d^{LV} \cos\Theta_d + \gamma_d^{SL}. \end{aligned} \tag{2}$$

SV, LV, SL, d, and f label the various interfaces between solid (S), air (vapor = V), and liquid (L) phases, respectively, droplet (d), and film (f) regimes. According to the

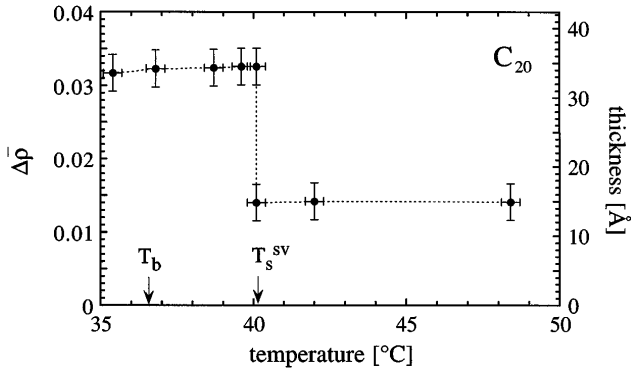

FIG. 4. Ellipsometric data from adsorption experiments of C_{20} onto SiO_2 (stepwise temperature increase, equilibrium data). $\Delta\bar{\rho}$ is the difference in ellipticity between bare and coated surfaces. The thicknesses are calculated with an assumed isotropic refractive index of 1.45.

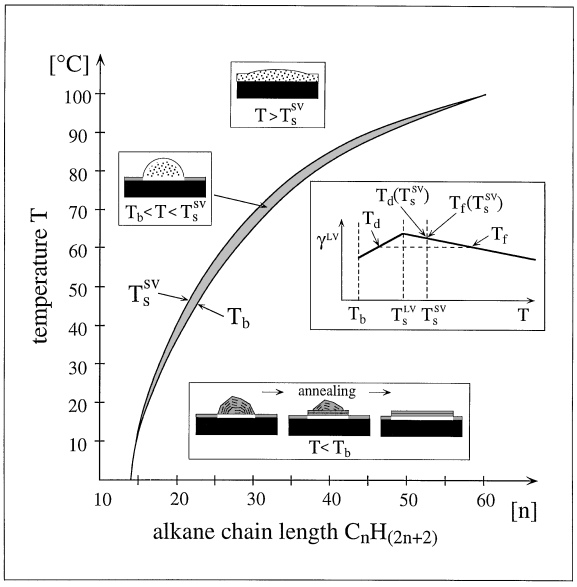

FIG. 5. Wetting regimes, topologies, and suggested molecular orderings as a function of the temperature and the chain length. The inset shows a schematic of the change of the surface tension γ^{LV} with temperature [9] including an example of T_f and T_d which matches Eq. (3) and the specific pair $T_d(T_S^{SV})$ and $T_f(T_S^{SV})$ to calculate $\Delta\gamma_{f,d}^{SV}(T_S^{SV})$. White fillings of interfaces indicate uncertainties in the molecular ordering.

literature [9], γ^{LV} varies with temperature near T_S^{SV} as shown in the inset of Fig. 5. From that is evident that corresponding temperatures T_d and T_f below and above T_S^{LV} can be found so that

$$\gamma_d^{LV}(T_d) = \gamma_f^{LV}(T_f) = \gamma^{LV}(T_d, T_f). \quad (3)$$

With Eq. (2) then follows

$$\gamma_f^{SV}(T_f) - \gamma_d^{SV}(T_d) = \gamma^{LV}(T_f, T_d)[\cos\Theta_f - \cos\Theta_d] + \gamma_f^{SL}(T_f) - \gamma_d^{SL}(T_d). \quad (4)$$

If we select T_d and T_f arbitrarily close to T_S^{SV} [i.e., $T_d(T_S^{SV})$ and $T_f(T_S^{SV})$ in the schematic], then $\gamma_f^{SL}(T_f) - \gamma_d^{SL}(T_d) = 0$ if we agree, as discussed already, that there is no discontinuous change of γ^{SL} at T_S^{SV}. We, thus, can estimate $\Delta\gamma_{f,d}^{SV}(T_S^{SV}) \approx 0.02$ mN/m with $\Theta_d = 2°$, $\Theta_f \approx 0°$, and $\gamma^{LV}(T_f, T_d) = 28$ mN/m [9].

The observed dewetting below T_S^{SV} is in qualitative agreement with adsorption studies of alkanes on Langmuir monolayers which consisted of amphiphiles with their alkane chains oriented towards the air [16]. Upon loosely packed, disordered monolayers, alkanes adsorb, whereas on densely packed, condensed monolayers, barely any alkane molecules are found.

Surface freezing has been explained theoretically [17] as the result of an additional fluctuation-based entropic contribution to the excess surface free energy. The molecules are ordered homeotropically and fluctuate normal to the interface. Our findings of monolayers slightly thicker than the molecular length as well as the similarities of the chain length and temperature dependency of $T_S^{SV} - T_b$ with those predicted by the theory and measured at alkane/air interfaces corroborate the theoretical approach. Minor discrepancies like the slightly extended temperature range ($T_S^{SV} \approx T_S^{LV} + 0.5$ °C) and monolayer thicknesses matching the molecular lengths at $C_n > C_{30}$ may be due to the different interfaces, respectively, molecular tilt.

Above T_S^{SV}, liquid alkane films much thicker than the molecular length are found. The thickness uniformity of these films, as well as those of the mesas at $T < T_b$, will be the subject of a different publication. Very similar mesa topologies with a tendency to height uniformity have been observed before for fatty acids [18] and explained as a consequence of the competition between short and long range forces.

Figure 5 graphically summarizes the three different wetting regimes and topologies as a function of the alkane chain length and the temperature. It is suggested that the decoupling of the phase transition temperatures of the bulk material at T_b and of the alkanes adjacent to the solid/vapor interface at T_S^{SV} causes the intermediate wetting regime between T_b and T_S^{SV}. The discontinuity of the surface energy γ^{SV} due to monolayer melting at T_S^{SV} can be estimated to be very small [$\Delta\gamma^{SV}(T_S^{SV}) \approx 0.02$ mN/m]. The monolayer freezing behavior at the substrate/air interface resembles that of surface freezing at liquid bulk alkane/air interfaces. This and other experimental findings support a fluctuation-stabilized surface freezing mechanism.

We thank Wacker Siltronic GmbH Burghausen for grateful donation of the silicon wafers. The work was supported by the Deutsche Forschungsgemeinschaft through Sfb 335.

[1] S. Dietrich, *Phase Transitions and Critical Phenomena*, edited by C. Domb and J. Lebowitz (Academic Press, London, 1988), Vol. 12.
[2] P. G. de Gennes, Rev. Mod. Phys. **57**, 827 (1985).
[3] W. H. Lawnik *et al.*, Langmuir **11**, 3075 (1995).
[4] M. L. Gee, T. W. Healy, and L. R. White, J. Colloid Interface Sci. **131**, 18 (1988).
[5] L. J. M. Schlangen *et al.*, Langmuir **11**, 1701 (1995).
[6] J. C. Berg, *Wettability*, edited by J. C. Berg (Dekker, New York, 1993).
[7] F. Brochart-Wyart and J. Daillant, Can. J. Phys. **68**, 1084 (1990); F. Brochart-Wyart *et al.*, Langmuir **7**, 335 (1991); G. J. Hirasaki, *Contact Angle, Wettability and Adhesion*, edited by K. L. Mittal (VSP, Utrecht, The Netherlands, 1993), p. 183.
[8] I. M. Tidswell *et al.*, Phys. Rev. B **44**, 10 869 (1991).
[9] X. Z. Wu *et al.*, Science **261**, 1018 (1993); Phys. Rev. Lett. **70**, 958 (1993); G. A. Sefler *et al.*, Chem. Phys. Lett. **235**, 347 (1995).
[10] T. Pfohl, D. Beaglehole, and H. Riegler, Chem. Phys. Lett. **260**, 82 (1996).
[11] K.-H. Graf and H. Riegler, Colloids and Surfaces A (to be published).
[12] A. Asmussen and H. Riegler, J. Chem. Phys. **104**, 8159 (1996).
[13] A. I. Kitaigorodskii, *Molecular Crystals and Molecules* (Academic Press, New York, 1973); X. Y. Liu and P. Bennema, J. Appl. Crystallogr. **26**, 229 (1993).
[14] C. Merkl (to be published).
[15] Annealed samples with mesas also show Bragg peaks. The internal layering is presumably parallel to the interface with bulk material spacings [13], which are different from those of the monolayers. The reflectograms of Fig. 3 stem from (unannealed) frozen droplets where the Bragg peaks are suppressed due to a randomly oriented microcrystalline structure.
[16] M. Thoma *et al.*, Langmuir **12**, 1722 (1996).
[17] A. V. Tkachenko and Y. Rabin, Phys. Rev. Lett. **76**, 2527 (1996).
[18] H. Riegler *et al.*, *Short and Long Chains at Interfaces*, edited by J. Daillant, P. Guenoun, C. Marques, P. Muller, and J. Tranh Thanh Van (Edition Frontieres, Gif-Sur-Yvette, France, 1995), p. 307.